Activity-based protein profiling in drug-discovery

Esbroeck, A.C.M. van

4

Activity-based protein profiling reveals off-target proteins of FAAH inhibitor BIA 10-2474

A.C.M. van Esbroeck
A.P.A. Janssen
A.B. Cognetta III
D. Ogasawara
G. Shpak
M. van der Kroeg
V. Kantae
M.P. Baggelaar
F.M.S. de Vrij
H. Deng
M. Allarà
F. Fezza
Z. Lin
T. van der Wel
M. Soethoudt
E.D. Mock
H. den Dulk
I.L. Baak
B.I. Florea
G. Hendriks
L. de Petrocellis
H.S. Overkleeft
T. Hankemeier
C.I. de Zeeuw
V. Di Marzo
M. Maccarrone
B.F. Cravatt
S.A. Kushner
M. van der Stelt

ABSTRACT | A recent phase I trial of the fatty acid amide hydrolase (FAAH) inhibitor BIA 10-2474 led to the death of one volunteer and produced mild-to-severe neurological symptoms in four others. Although the cause of the clinical neurotoxicity is unknown, it has been postulated that, given the clinical safety profile of other tested FAAH inhibitors, off-target activities of BIA 10-2474 may have played a role. The BIA 10-2474 interaction landscape was determined by activity-based proteomics and revealed that the drug inhibits several lipases that are not targeted by PF04457845, a highly selective and clinically tested FAAH inhibitor. BIA 10-2474, but not PF04457845, produced substantial alterations in lipid networks in human cortical neurons, suggesting that promiscuous lipase inhibitors have the potential to cause metabolic dysregulation in the nervous system.

Published as part of Van Esbroeck et. al., *Science,* 2017

Introduction

Severe adverse effects of drug candidates are rarely observed in phase I clinical trials, due to extensive preclinical toxicological profiling in animals and precautions taken into account in the design of first-in-human studies. However, in January 2016, a first-in-human study of the fatty acid amide hydrolase (FAAH) inhibitor BIA 10-2474 led to the death of one volunteer and the hospitalization of four others[1–4]. All patients manifested mild-to-severe neurological symptoms[3]. In rodents, no obvious toxicological results were found with BIA 10-2474 that could predict the observed human clinical neurotoxicity. In a study on dogs treated for 13 weeks with BIA 10-2474, a dose-dependent pulmonary toxicity was observed and two dogs from the subgroup receiving the highest dose were sacrificed[4]. An initial toxicology study in primates showed that the highest administered dose led to axonal dystrophy in the spinal bulb. A follow-up primate study led to the death of one animal and the sacrifice of several others for undisclosed ethical reasons[4]. However, these findings were not considered to be sufficiently concerning to abandon the first-in-human studies due to the large therapeutic window in preclinical studies of BIA 10-2474.

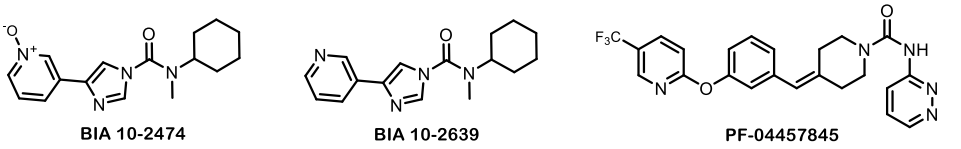

Figure 1 | Chemical structures of FAAH inhibitor BIA 10-2474, its metabolite BIA 10-2639, and clinically safe FAAH inhibitor PF04457845.

The BIA 10-2474 target enzyme FAAH is a membrane-bound serine hydrolase that degrades the endocannabinoid anandamide and related amidated lipids[5–8]. Three explanations for the clinical neurotoxicity of BIA 10-2474 have been proposed: (I) errors may have occurred in the clinical trial itself, either in the manufacturing or handling of the compound or in the conduct of the trial; (II) through its inhibitory effects on FAAH, BIA 10-2474 may have produced high levels of long-chain fatty acid amides (e.g. anandamide) and their oxygenated metabolites, which could potentially overstimulate cannabinoid CB1R[8], TRPV1[9], and/or NMDA receptors[10]; or (III) BIA 10-2474 and/or its metabolites might have off-target activities. The first hypothesis was dismissed by the French authorities[4]. The second hypothesis is considered unlikely because other FAAH inhibitors, such as PF04457845, have exhibited favorable safety profiles in phase I and II clinical trials[11,12]. The third hypothesis has not been directly evaluated, because little or no information was available regarding the protein interaction profile of BIA 10-2474[1].

BIA 10-2474 (Figure 1) contains an electrophilic imidazole urea that may react with the nucleophilic serine of FAAH and other serine hydrolases to form covalent and irreversible adducts. Based on previously developed chemical proteomic methods to map the interaction landscapes of (ir)reversible serine hydrolase inhibitors[13–15], it was anticipated that the serine hydrolase targets of BIA 10-2474 could be identified and

compared to the selectivity profiles of clinical FAAH inhibitor PF04457845 (Figure 1), which has progressed to phase II trials without any serious adverse events[16]. BIA 10-2639, a confirmed metabolite in which the *N*-oxide is reduced to a pyridine (Figure 1)[4] was investigated to compare inhibitor and metabolite activity.

The interaction landscape of BIA 10-2474 was investigated by activity-based protein profiling (ABPP), a chemical proteomic method that employs active site-directed chemical probes to record the functional state of entire enzyme classes directly in native biological systems[13–15]. When coupled to fluorescent reporter groups, activity-based probes (ABPs) enable convenient visualization of enzyme activities in complex proteomes by SDS-PAGE (sodium dodecyl sulfate polyacrylamide gel electrophoresis) and in-gel fluorescence scanning. When coupled to a biotin reporter group, ABPs enable affinity enrichment and identification of enzyme activities by mass spectrometry (MS)-based proteomics. In either format, ABPP serves as a versatile method to assess target engagement and proteome-wide selectivity for small-molecule inhibitors as pre-incubation of the proteome with an inhibitor will reduce the ABP labeling of proteins targeted by the inhibitor.

Results

BIA 10-2474 is a weak irreversible inhibitor of FAAH and ABHD6 *in vitro*

Competitive and comparative gel-based ABPP was performed using two different probes: the broad spectrum serine hydrolase-directed fluorophosphonate-rhodamine (FP-TAMRA) and the tailored β-lactone probe MB064 that preferentially reacts with endocannabinoid related hydrolases diacylglycerol lipase α (DAGLα), α/β hydrolase domain containing protein 6 (ABHD6) and 12 (ABHD12), along with a handful of other enzymes[14]. Together, FP-TAMRA and MB064 provided a target engagement assay for FAAH and a broad array (>50) of other brain serine hydrolases.

Human frontal cortex (GFi3) and cerebellum samples were acquired from three male donors (aged 49, 50, and 80 years old with a post-mortem delay of 4-8 h) without any history of neuropsychiatric illness or postmortem evidence of neuropathology. ABPP studies revealed that the membrane and soluble serine hydrolase content were overlapping but varied between these brain regions (Supplementary Figure S1). The identity of FAAH and other endocannabinoid hydrolases including DAGLα and ABHD6 was confirmed with reference inhibitors by competitive ABPP (Supplementary Figure S2). In total, 49 and 56 fluorescent bands corresponding to putative serine hydrolases were detected in frontal cortex (Figure 2A-D) and cerebellum (Supplementary Figure S3A-D) respectively.

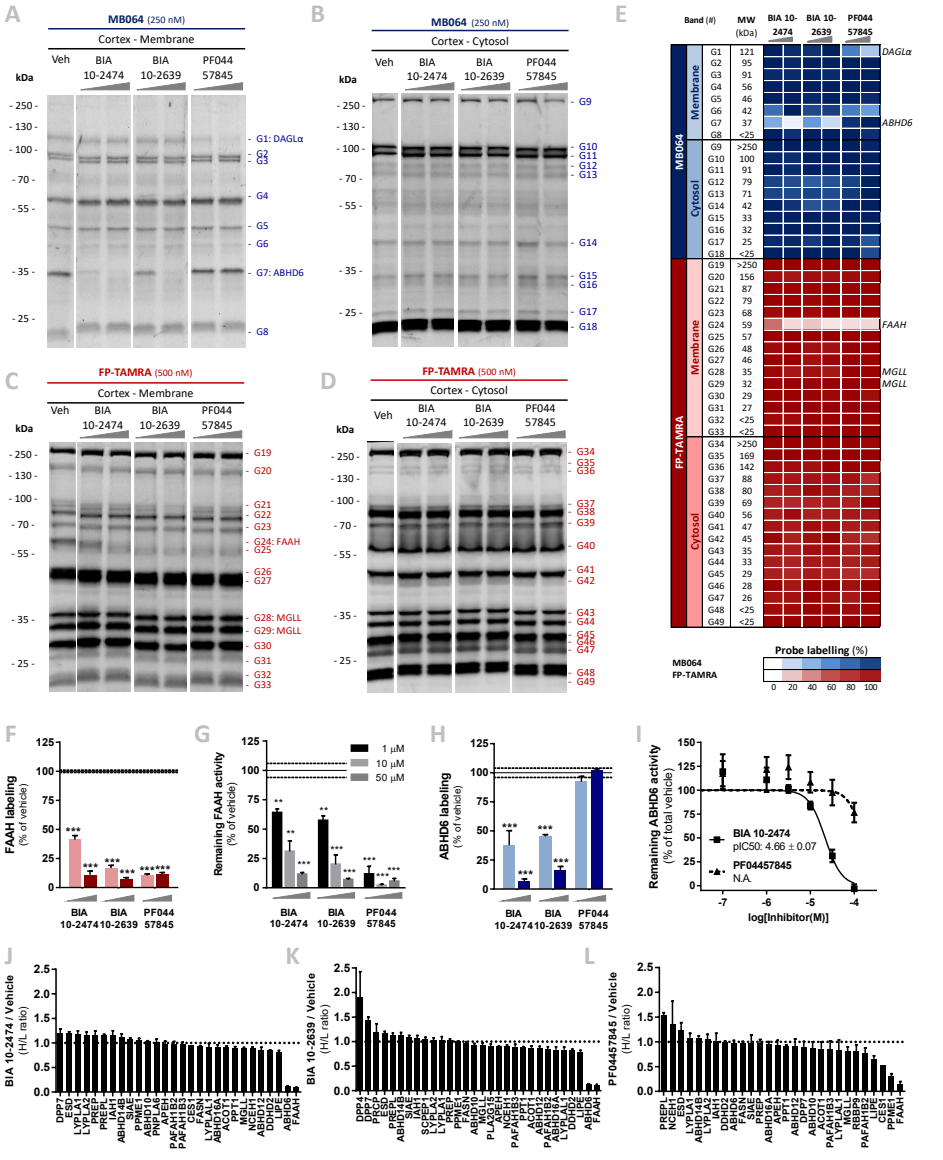

Figure 2 | Identification of FAAH and ABHD6 as *in vitro* targets of BIA 10-2474 by competitive ABPP on serine hydrolases. (**A**-**F**, **H**) Gel-based ABPP analysis of human cortex (GFi3) proteome incubated *in vitro* with vehicle or inhibitor BIA 10-2474, BIA 10-2639 or PF04457845 (10/50 μM, 30 min, 37 °C) and subsequently labeled with MB064 (250 nM) (**A**, **B**) or FP-TAMRA (500 nM) (**B**, **D**) (20 min, rt). The serine hydrolase activities were quantified, normalized for protein loading and expressed relative to control. Heat-map summary of all 49 quantified bands (**E**) and bar-graph depiction of BIA 10-2474 (off-)targets FAAH (**F**) and ABHD6 (**H**). (**G**) FAAH activity relative to vehicle treated control after incubation with BIA 10-2474, BIA 10-2639 or PF04457845 (1/10/50 μM,15 min, rt) as measured in a radiometric [^{14}C]-anandamide assay on purified recombinant FAAH. (**I**) Dose response curve of BIA 10-2474 and PF04457845 on recombinant ABHD6, as measured in a natural substrate assay. (**J**-**L**) Chemical proteomics analysis of human cortex (GFi3 proteome), treated with BIA 10-2474 (**J**), BIA 10-2639 (**K**), or PF04457845 (**L**) (50 μM, 30 min, 37 °C) using probes MB108 or FP-biotin (10 μM, 60 min, rt). Data is expressed as a H/L ratio as compared to vehicle treated sample. (**E**-**L**) Data is expressed as mean ± SEM (**E**-**H**, **J**-**L**: n=3, **K**: n=4) with * $p < 0.05$, ** $p < 0.01$, *** $p < 0.001$ (two-tailed *t*-test).

The clinical trial subjects who developed neurological symptoms were exposed to a dosage of BIA 10-2474 that was 10 to 50 times higher than that required for blockade of FAAH activity in the clinical trial participants[4]. Inhibitor activity against FAAH and other serine hydrolases was therefore evaluated at two high concentrations (10 and 50 µM) in human brain soluble and membrane proteomes by gel-based competitive ABPP. Representative gel-based ABPP data are shown (Figure 2A-D, Figure 2A-D) alongside a heat map that summarizes the inhibitor-serine hydrolase interaction landscape (Figure 2E, Supplementary Figure S3E).

BIA 10-2474, BIA 10-2639, and PF04457845 all inhibited FAAH, with BIA 10-2474 showing the weakest inhibitory effect (Figure 2F). In a radioactive substrate assay using [^{14}C]-anandamide, the weak inhibitory activity of BIA 10-2474 and BIA 10-2639 was confirmed with IC_{50} values > 1 µM as compared to ± 0.01 µM for PF04457845 (Figure 2G). Notably, BIA 10-2474 as well as its metabolite exhibited distinct off-target activity towards ABHD6 in the gel-based assay (Figure 2H), which was not observed for PF04457845. Moreover, BIA 10-2474 and its metabolite did not reduce the labeling of endocannabinoid hydrolases monoacylglycerol lipase (MGLL) and DAGLα (Figure 2E, Supplementary Figure S3E).

The brain off-target profiles of FAAH inhibitors were confirmed and extended by performing ABPP coupled to high-resolution quantitative mass spectrometry (MS). This methodology allows for a more accurate quantification by avoiding the band overlap observed with the gel-based assays and enables screening of the inhibitors over a broader range of serine hydrolases. Quantitative MS confirmed complete inhibition of FAAH and validated ABHD6 as an off-target of BIA 10-2474 and its metabolite, but not of PF04457845 (Figure 2J-L). PPME1 was identified as a potential off-target of PF04457845 with a heavy/light ratio < 0.5 (Figure 2L).

To confirm that the off-target ABHD6 identified by ABPP was inhibited in its catalytic activity, its activity was measured in a real-time fluorescence-based natural substrate assay[17]. BIA 10-2474 inhibited recombinant ABHD6-mediated hydrolysis of 2-AG with an IC_{50} of 22 ± 4 µM (n=4), whereas PF04457845 was inactive (IC_{50} > 100 µM) (Figure 2I). Notably, BIA 10-2474, BIA 10-2639 and PF04457845 did not cross-react with other proteins of the endocannabinoid system including DAGLα, DAGLβ, MGLL and *N*-acyl phosphatidylethanolamine phospholipase D (NAPE-PLD), nor with the endocannabinoid-binding TRP ion channels (Supplementary Tables S1, S2).

The BIA 10-2474 interaction profiling was extended with three compounds in which an alkyne functionality was introduced at different positions in the molecule (AJ167, AJ179, AJ198) (Supplementary Figure S4A)[18]. The alkyne group serves as a ligation handle to introduce fluorescent reporter groups via copper(I)-catalyzed azide-alkyne cycloaddicition ("click") chemistry[19]. Few additional labeled proteins were detected in human cortical and cerebellar proteomes (Supplementary Figure S4E-G) for which no competition was observed upon pre-incubation with BIA 10-2474, indicating limited

cross-reactivity of BIA 10-2474 with non-serine hydrolases in the brain proteome. Importantly, these experiments definitively prove covalent binding of AJ179 and AJ198 to FAAH (Supplementary Figure S4B-C, E-F), which was maintained even under denaturing SDS-PAGE conditions, thereby supporting an irreversible reaction mechanism for BIA 10-2474.

BIA 10-2474 inhibitory potency is drastically improved *in situ*

As noted above, in the biochemical substrate assay using recombinant FAAH and gel-based ABPP experiments with human brain lysates, BIA 10-2474 exhibited weaker *in vitro* potency for FAAH compared to PF04457845. Notably, this difference was attenuated *in situ*, as our gel-based ABPP experiments revealed that BIA 10-2474 inhibited FAAH, as well as other serine hydrolases (e.g., ABHD6 and FAAH2, which is a human-specific orthologue of FAAH[20]) with substantially increased potency in human cells (Figure 3). The reason for the increased cellular activity of BIA 10-2474 is at present unclear, but it was consistently observed in multiple cell types (data not shown) and with multiple protein targets of the compound, which may suggest that cellular accumulation of the compound results in greater than expected inhibitory activity against FAAH and other serine hydrolases. Previous chemical proteomic studies have uncovered similar effects for covalent kinase inhibitors[21].

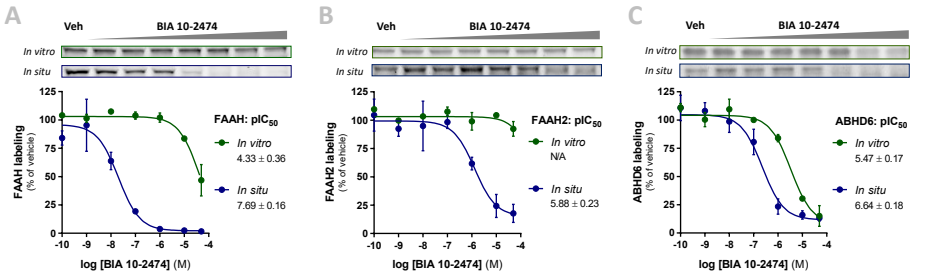

Figure 3 | BIA 10-2474 inhibitory potency towards FAAH, FAAH2, and ABHD6 is increased *in situ*. (**A**-**C**) Dose response curves of BIA 10-2474 against FAAH, ABHD6 and FAAH2 *in vitro* and *in situ*. HEK293-T cells transiently overexpressing FAAH (**A**) or FAAH2 (**B**), or endogenously expressing ABHD6 (**C**) were treated *in situ* with vehicle or BIA 10-2474 (0.1 nM – 50 µM, 2 h, 37 °C), harvested and subsequently prepped as whole lysates (*in situ* samples, blue). Alternatively, membrane fractions from HEK293-T cells overexpressing recombinant FAAH and FAAH2 were mixed and *in vitro* incubated with vehicle of BIA 10-2474 (0.1 nM – 50 µM, 30 min, 37 °C) (*in vitro* samples, green). Subsequently, all samples were labeled with activity-based probe FP-TAMRA (500 nM, 20 min, RT). Remaining probe labeling was quantified, normalized for protein loading and expressed relative to vehicle treated sample. Data is expressed as mean ± SEM (Vehicle: n=6, BIA: n=3) and pIC_{50+} ± SD.

BIA 10-2474 disrupts the neural lipid network by targeting multiple hydrolases

In light of the increased *in situ* potency of BIA 10-2474, its off-target profile was investigated in human cortical neurons using gel-based ABPP studies. Apart from FAAH and ABHD6, three additional targets were identified with molecular weights of approximately 150, 62 and 47 kDa respectively (Figure 4A). Using chemical proteomics,

these off-targets were confirmed and identified as patatin-like phospholipase domain containing protein 6 (PNPLA6, also known as neuropathy target esterase (NTE)), carboxyl esterase 2 (CES2) and phospholipase 2 group XV (PLA2G15, also known as phospholipase A2 (LPLA2)) with a heavy/light ratio < 0.5 (Figure 4B).

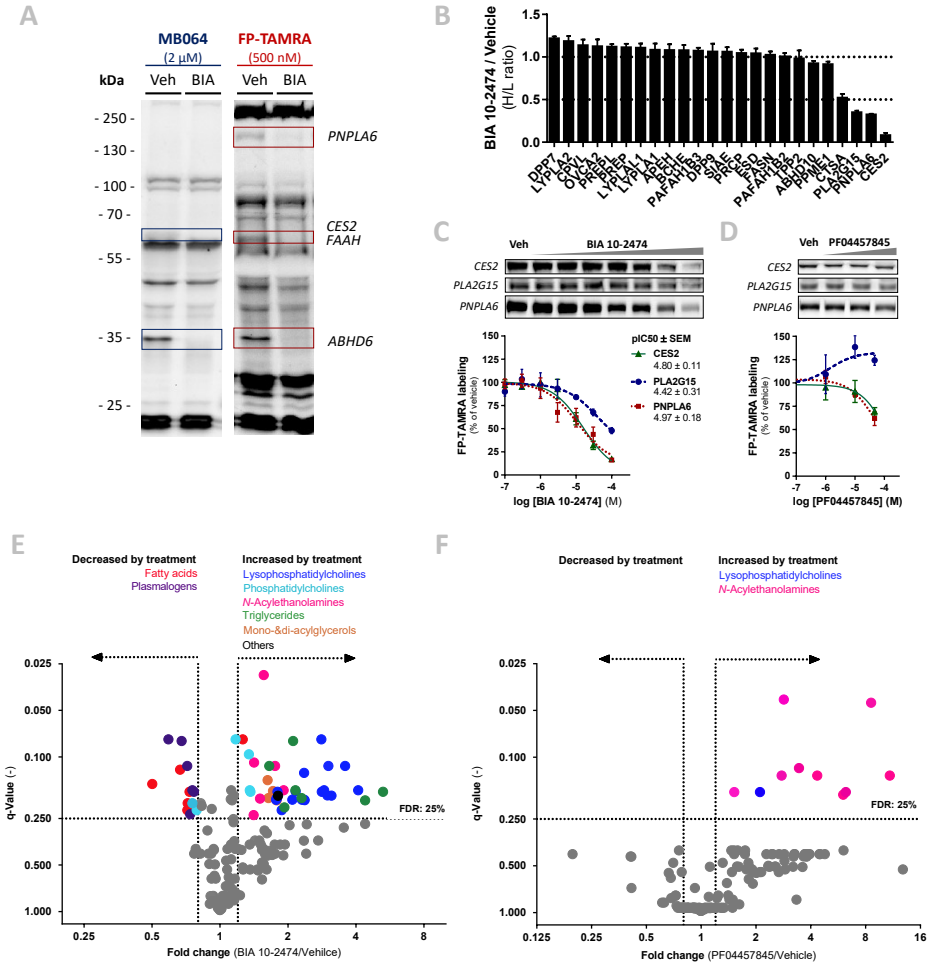

Figure 4 | *In situ* treatment of human neuronal cultures with BIA 10-2474 reveals additional off-targets and results in disruption of lipid homeostasis. (**A**-**B**) Human neuronal cultures were treated *in situ* with vehicle or BIA 10-2474 (50 µM, 24 h, 37 °C). Lysates were labeled with activity-based probes MB064 (2 µM) or FP-TAMRA (500 nM) (20 min, rt) for gel-based ABPP (**A**) or with MB108 or FP-biotin (10 µM, 60 min, rt) for chemical proteomics (**B**). (**C**-**D**) Dose response curves of BIA 10-2474 against CES2, PLA2G15 or PNPLA6 *in situ*. HEK293-T cells transiently overexpressing CES2, PLA2G15, or PNPLA6 were treated *in situ* with vehicle, BIA 10-2474 (0.1-100 µM) (**C**), or PF04457845 (0.1 – 50 µM) (**D**) (24 h, 37 °C). Whole lysates were labeled with activity-based probe FP-TAMRA (500 nM, 20 min, rt). Remaining probe labeling was quantified, normalized for protein loading and expressed relative to vehicle treated sample. Data is expressed as mean ± SEM (vehicle: n=6, treated: n=3) and pIC_{50} ± SD. (**E**-**F**) Volcano plot of lipidomics analysis of human neurons treated *in situ* with vehicle, BIA 10-2474 (50 µM) (**E**), or PF04457845 (1 µM) (**F**) (48 h, 37 °C). Lipids with a fold change (FC) threshold of ≥1.20 or ≤0.80 and Benjamini–Hochberg false discovery rate (FDR) ≤ 25% are represented by colored circles distinguished by lipid class (n=3).

Most of the interaction partners of BIA 10-2474 identified in this study are known to be involved in cellular lipid metabolism[22,23]. To confirm the interaction of BIA 10-2474 with its lipolytic serine hydrolase off-targets, these proteins were transiently overexpressed in HEK293-T cells and concentration-dependent *in situ* inhibition was assessed using gel-based ABPP (Figure 4C-D). BIA 10-2474, but not PF04457845, inhibits PNPLA6, CES2 and PLA2G15 with IC_{50}-values of 11, 16 and 38 µM respectively.

Based on the off-target profile of BIA 10-2474 it was postulated that prolonged exposure to BIA 10-2474 might result in alterations of human neuronal lipid metabolism. This hypothesis was tested by targeted lipidomics analysis of human cortical neurons treated with vehicle or BIA 10-2474. In total, 161 lipid species were quantified from which significant changes in several lipid classes were observed. Levels of *N*-acylethanolamines, triglycerides, monoacylglycerols, and (lyso)phophatidylcholines were increased in BIA 10-2474-treated cells, while those of free fatty acids and plasmalogens were reduced, consistent with the inhibition of FAAH, FAAH2, ABHD6, CES2, PLA2G15, and PNPLA6 activities (Figure 4E). Prolonged treatment with PF04457845 only affected lipid levels of a lysophosphatidylcholine and increased several *N*-acylethanolamines, consistent with FAAH and FAAH2 inhibition (Figure 4F).

Discussion

No information had previously been available regarding the protein interaction profile of BIA 10-2474 that could help in defining the cause of its clinical toxicity, and in particular to directly evaluate the possibility that the observed clinical neurotoxicity might have resulted from off-target activity[1]. Aided by chemical proteomic methods for mapping the interaction landscapes of serine hydrolase inhibitors[13–15,24,25], the serine hydrolase target selectivity of BIA 10-2474 was compared to that of PF04457845, a widely used clinically safe FAAH inhibitor. Here, BIA 10-2474 was shown to be an irreversible, potent FAAH and FAAH2 inhibitor *in situ,* that increases cellular levels of long-chain fatty acid ethanolamines. Using human brain tissue lysates and cultured human cortical neurons and cell lines, multiple lipase off-targets of BIA 10-2474 (including ABHD6, CES2, PLA2G15 and PNPLA6) were discovered that were not targeted by PF04457845. By targeting these lipases, BIA 10-2474 disrupted the neural lipid metabolism, resulting in increased levels of *N*-acylethanolamines, monoacylglycerols, triglycerides, (lyso)phosphatidylcholines, and reductions in free fatty acids and plasmalogens. When considering the basis for BIA 10 2474's broader interaction profile with serine hydrolases compared to PF04457845, the greater intrinsic reactivity of BIA 10-2474, which is reflected in a much faster rate of methanolysis (data not shown), may have been a contributing factor.

FAAH2 is a human orthologue of FAAH, which also degrades long-chain fatty acid amides[20]. However, little is known about the neurobiological function of FAAH2. CES2 is a serine esterase involved in the hydrolysis of ester and amide bonds of xenobiotics and prodrugs, but also of endogenous lipids. It is highly expressed in the liver and in

endothelial cells. Hepatic CES2 is required for triglyceride homeostasis by modulating lipolysis, ER stress and lipogenesis[26]. PLA2G15 is a lysosomal phospholipase highly expressed in alveolar macrophages and microglial cells. Inhibition of PLA2G15 leads to accumulation of phosphatidylcholines and phosphatidylethanolamines, and has previously been implicated in drug-induced phospholipidosis[27].

ABHD6 has a minor role in endocannabinoid 2-arachidonoylglycerol (2-AG) metabolism[28], degrades bis(monoacylglycerol)phosphate[29], and acts as a lysophosphatidyl hydrolase[22,28]. Independent of its catalytic function, ABHD6 exhibits a scaffolding function. Recently, proteomic experiments revealed that ABHD6 physically interacts with the C-terminal tail of the GluR1 subunit of the α-amino-3-hydroxy-5-methyl-4-isoxazolepropionic acid receptor (AMPAR), one of the major postsynaptic ionotropic glutamate receptors mediating excitatory synaptic neurotransmission in the central nervous system. Two independent groups have shown that ABDH6 is a potent negative regulator of cell surface trafficking of GluR1-containing AMPARs[30,31]. Some enzyme inhibitors are known to act as chemical chaperones increasing cellular protein levels by reducing proteolysis or enhancing protein biosynthesis and folding[32]. BIA 10-2474 might also act as a chemical chaperone to modulate ABHD6 protein levels, thereby possibly affecting AMPAR signaling in neuronal tissue.

PNPLA6 has previously been linked to neurodegeneration in humans resulting from organophosphate-based pesticides[23,33]. PNPLA6 is a (lyso)phospholipase that uses (lyso)phosphatidylcholine as a substrate and is highly expressed in endothelial cells, astrocytes, and neurons. Proper neuronal phosphatidylcholine homeostasis mediated by PNPLA6 is required for axonal maintenance[34]. PNPLA6 inhibition leads to neurodegeneration following an age-dependent neuropathy of increasing severity in older age. Notably, PNPLA6-mediated neurotoxicity following acute organophosphate exposure is species dependent, with less pronounced effects in rodents than humans. Mice with a homozygous germline deletion of PNPLA6 have embryonic lethality due to placental and vasculature defects, however, brain-specific deletion of PNPLA6 results in prominent neuronal pathology[35]. A threshold of > 70% PNPLA6 inhibition has been determined as responsible for developing neurodegeneration upon organophosphate exposure in chicken[23,33]. It is remarkable that many clinical symptoms arising from PNPLA6-mediated neurological sequelae following organophosphate exposure resemble the neuropathology observed in the clinical trial participants[3] who received a cumulative dose of 250-300 mg of BIA 10-2474, including precedent for human neurotoxicity, brain region sensitivity, age dependency, species selectivity, dosing threshold and time course of neuropathology. Additional experimental evidence and more detailed information from the Rennes' clinical trial will be required to firmly establish the relative causality of the identified BIA 10-2474 off-targets. Importantly, based on this work it cannot be excluded that non-covalent interactions of BIA 10-2474 may have contributed to the drug's neurotoxic effects.

Conclusion

Taken together, this study shows that BIA 10-2474 is a covalent irreversible and non-selective serine hydrolase inhibitor and highlights the disruption of cellular lipid networks as an important potential mediator of the observed neurotoxicity. The described data do not reveal whether inhibition of one or more of the identified BIA 10-2474's off-target proteins (including FAAH2, ABHD6, PNPLA6, PLA2G15 and CES2) are responsible for the clinical neurotoxicity caused by this drug. However, the study does emphasize the general utility of ABPP as a versatile chemical proteomic method to assess on-target engagement and off-target activity of covalent drugs to guide therapeutic development. In retrospect, it appears likely that the implementation of a method such as ABPP might have permitted a safer clinical trial design for BIA 10-2474 by establishing a dose range in which FAAH was inhibited, but still below the threshold for engaging off-target interactions.

Experimental procedures

Materials, probes and inhibitors

Activity-based probe TAMRA-fluorophosphonate (FP-TAMRA) was purchased from ThermoFisher, MB064 and MB108 were synthesized in-house as previously described[24]. PF04457845 was synthesized in house, as well as purchased from Sigma Aldrich. Inhibitors BIA 10-2474, BIA 10-2639 and activity-based probes AJ167, AJ179, AJ198 were synthesized in-house as previously described[18]. All synthesized compounds were at least 95% pure and were analyzed by LC-MS, NMR and HRMS. Other chemicals, reagents, and primers were purchased from Sigma Aldrich unless indicated otherwise.

Cloning

Full-length human cDNA of ABHD6, FAAH, PNPLA6, PLA2G15, CES2 (Source Bioscience) and FAAH2 (BioCat) was cloned into mammalian expression vector pcDNA3.1, containing genes for ampicillin and neomycin resistance. The inserts were cloned in frame with a C-terminal FLAG-tag and site-directed mutagenesis was used to remove restriction sites by silent point mutations. Plasmids were isolated from transformed XL-10 Z-competent cells (Maxi Prep kit: Qiagen) and sequenced at the Leiden Genome Technology Center. Sequences were analyzed and verified (CLC Main Workbench).

Cell culture

General

HEK293-T (human embryonic kidney) cells were cultured at 37 °C under 7% CO_2 in DMEM containing phenol red, stable glutamine, 10% (v/v) new born calf serum (Thermo Fisher), and penicillin and streptomycin (200 µg/mL each; Duchefa). Medium was refreshed every 2-3 days and cells were passaged twice a week at 80-90% confluency by resuspension in fresh medium. Cell lines were purchased from ATCC and were regularly tested for mycoplasma contamination. Cultures were discarded after 2-3 months of use.

Human neural cell culture

Human iPSC-derived neural progenitor cells (NPCs) (Axol Biosciences, line ax0015) were plated on sterile coverslips in 12-well plates, coated with poly-L-ornithin/laminin (Sigma-Aldrich), in neural differentiation medium (Neurobasal medium, 1% N2 supplement, 2% B27-RA supplement, 1% MEM-NEAA, 20 ng/mL BDNF (ProSpec Bio)), 20 ng/mL GDNF (ProSpec Bio), 1 µM db-cAMP (Sigma-Aldrich), 200 µM ascorbic acid (Sigma-Aldrich), 2 µg/mL laminin, and 1% P/S), resulting in neural networks composed of neurons and glia. Cells were refreshed with neural differentiation medium 3 times per week. During weeks 1-4, medium was fully refreshed. After 4 weeks of neural differentiation, only half of the volume of medium per well was refreshed.

Transient Transfection

One day prior to transfection HEK293-T cells were seeded to 15 cm dishes or 12 wells plates (~62.500 cells/cm^2). Prior to transfection, culture medium was aspirated and a minimal amount of medium was added. A 3:1 (m/m) mixture of polyethylenimine (PEI) (60 µg/dish or 1.875 µg/well) and plasmid DNA (20 µg/dish or 0.625 µg/well) was prepared in serum free culture medium and incubated (15 min, rt). Transfection was performed by dropwise addition of the PEI/DNA mixture to the cells. Transfection with the empty pcDNA3.1 vector was used to generate control samples. After 24 h, medium was refreshed. Medium was aspirated 48 or 72 h post-transfection and cells were harvested by resuspension in PBS. Cells were pelleted by

centrifugation (5 min, 1,000 *g*) and the pellet was washed with PBS. Supernatant was discarded and cell pellets were frozen in liquid nitrogen and stored at -80 °C until sample preparation.

In situ treatment

In situ treatment was initiated 24 h (for 24-48 h treatment) or 48 h (for 2 h treatment) post-transfection in 12 wells plates. Medium was aspirated and medium containing inhibitor or DMSO as vehicle was added (0.1 - 1.0% DMSO, DMSO concentration constant within each experiment). Final concentrations for inhibitors are indicated in the main text and figure legends. After 2, 4, 24, or 48 h exposure to treatment medium, medium was aspirated and cells were harvested and stored as described above until sample preparation (whole cell lysate).

Sample preparation

Whole cell lysate

Cell pellets were thawed on ice, resuspended in cold lysis buffer (20 mM HEPES pH 7.2, 2 mM DTT, 250 mM sucrose, 1 mM $MgCl_2$, 2.5 U/mL benzonase) and incubated on ice (15 min). The cell lysate was used for membrane preparation (below) or was diluted to appropriate concentration in cold storage buffer (20 mM Hepes, pH 7.2, 2 mM DTT) for use as whole lysate (HEK293-T: 2.0 mg/mL, neuronal cultures: 1.5 mg/mL). Protein concentrations were determined by a Quick Start™ Bradford Protein Assay (Bio-Rad) and diluted samples were flash frozen in liquid nitrogen and stored at -80 °C until further use.

Tissue lysate

Human Brain Tissue was supplied by the Netherlands Brain Bank and stored at - 80 °C until use. Tissues were thawed on ice, dounce homogenized in cold lysis buffer (20 mM HEPES pH 7.2, 2 mM DTT, 250 mM sucrose, 1 mM $MgCl_2$, 2.5 U/mL benzonase) and incubated on ice (15 min), followed by two low-speed spins (3 min, 2500 *g*, 4 °C) to remove debris. The supernatant fraction was used for separation of the cytosolic and membrane fractions.

Membrane preparation from lysate

The membrane and cytosolic fractions of cell or tissue lysates were separated by ultracentrifugation (93,000 *g*, 45 min, 4 °C). The supernatant was collected (cytosolic fraction) and the membrane pellet was resuspended in cold storage buffer by thorough pipetting and passage through an insulin needle. Protein concentrations were determined by a Quick Start™ Bradford Protein Assay (Bio-Rad) and samples were diluted to 2.0 mg/mL with cold buffer (20 mM Hepes pH 7.2, 2 mM DTT), flash frozen in liquid nitrogen and stored at -80 °C until further use. FAAH and FAAH2 overexpression membranes were mixed in an appropriate ratio for ABPP (0.1 mg/mL : 1.0 mg/mL).

Activity-based protein profiling

Direct activity-based probes

Gel-based ABPP was performed and analyzed with minor adaptations on previously reported procedures[24]. In brief, for *in vitro* inhibition, human brain proteome or cell lysate was incubated with vehicle (2.5% DMSO) or inhibitor (final concentrations indicated in figure legends) (30 min, 37 °C), followed by an incubation with the activity-based probe MB064 (250 nM, 2 µM) or FP-TAMRA (500 nM) (20 min, rt). Lysates from *in situ* treated cells were directly incubated with activity-based probes. Reactions were quenched with Laemlli buffer (30 min, rt) and proteins (brain: 20 µg, HEK293-T: 10 µg, neurons: 7.5 µg) were resolved by SDS-PAGE (10% acrylamide gel, 180 V, 75-80 min). In-gel fluorescence was scanned using Cy3 and Cy5 multichannel settings (605/50 and 695/55 filters, respectively) on a ChemiDoc imaging system (Bio-Rad) and stained with coomassie after scanning. Fluorescence was normalized to coomassie staining and quantified

with ImageLab™ software (Bio-Rad). Data was processed in Excel (Microsoft) and graphs and IC_{50} fits were prepared with Graphpad Prism 7 (Graphpad).

Two-step activity-based probes

The two-step labeling was adapted from previously developed methods[36]. In brief, human brain proteome (80 µg in 40 µL, cytosol or membrane fraction) was pre-incubated with vehicle or inhibitor (50 µM, 30 min, 37 °C), followed by an incubation with the alkyne probe (50 µM, 30 min, 37 °C) and subsequent conjugation to Cyanine-5-azide (Cy5-N_3) by addition of 5 µL freshly prepared click mix (40 mM $CuSO_4 \cdot (H_2O)_5$, 240 mM sodium ascorbate, 0.3 mM THPTA, 35 µM Cy5-N_3) (60 min, rt). Proteins were precipitated by adding methanol (50 µL), chloroform (15 µL) and water (15 µL), mixed by brief vortexing and pelleted by centrifugation (10 min, 4000 rpm). The supernatant was removed and the pellet was washed twice with methanol (50 µL). The pellet was redissolved in Laemmli buffer (40 µL, 95 °C, 5 min) and 20 µg protein was resolved by SDS-PAGE (10% acrylamide gel, 180 V, 75-80 min). In-gel fluorescence was scanned using Cy3- and Cy5-multichannel settings (605/50 and 695/55 filters, respectively) on a ChemiDoc imaging system (Bio-Rad) and stained with coomassie after scanning.

Activity-based proteomics

Activity-based proteomics was based on previously described procedures[14]. In summary, human GFi3 proteome (250 µg protein from cytosolic or membrane fraction) or human neurons (90 µg protein from whole lysate, *in situ* vehicle or inhibitor treated) was incubated with vehicle (2% DMSO) or inhibitor (BIA 10-2474 or PF04457845, 50 µM, 30 min, 37 °C). The proteome was labeled with MB108 or FP-Biotin (10 µM, 60 min, rt). The labeling reaction was quenched and after a chloroform/methanol precipitation, the precipitated proteome was resuspended in 6 M Urea / 25 mM ammonium bicarbonate (15 min, rt). The proteome was reduced (10 µM DTT, 15 min, 65 °C), alkylated (iodoacetamide, 40 mM, 30 min, rt), and subsequently heated with SDS (0.2%, 5 min, 65 °C). Avidin-Agarose beads (50 µL of a 50% slurry / sample) were washed with PBS and incubated with the proteome (3 h, rt, shaking). Beads were isolated by centrifugation (2500 *g*, 2 min) and washed with SDS-PBS (0.5% w/v) once and three times with PBS. After transfer to a low-binding Eppendorf tube, proteins were digested with sequencing grade trypsin (Promega) (500 ng per sample) in 250 µL OB-Dig buffer (100 mM Tris pH 8.0, 100 mM NaCl, 1 mM $CaCl_2$, 2% acetonitrile) (37 °C, O/N, 900 rpm). The pH was adjusted with formic acid to pH 3 and beads were removed by filtration. Peptides were isotopically labeled by on stage-tip dimethyl labeling, with subsequent addition of 20, 20, 30, 30, and 40 µL of light (vehicle, L) or medium (inhibitor, H) reagent to the stage-tips. The centrifugation speed during labeling was adjusted to have a flow through time of approximately 5 min (400 - 1000 *g*) per labeling step.

Targeted lipidomics

Sample extraction

Lipids were extracted from *in situ* treated human neurons (48 h, 50 µM BIA 10-2474, 1 µM PF04457845 or vehicle (0.25% DMSO)). The sample extraction was performed on ice. In brief, cell pellets with 1 million cells were transferred to 1.5 mL Eppendorf tubes, spiked with 10 µL each of deuterated internal standard mix for endocannabinoids (*N*-arachidonoylethanolamide (AEA)-d8, *N*-arachidonoyldopamine (NADA)-d8, *N*-docosahexaenoylethanolamide (DHEA)-d4, 2-arachidonoylglycerol (2-AG)-d8, *N*-stearoylethanolamine (SEA)-d3, *N*-palmitoylethanolamine (PEA)-d4, *N*-linoleoylethanolamine (LEA)-d3 and *N*-oleoylethanolamine (OEA)-d4), positive apolar lipids (lysophosphatidylcholines (LPC)17:0, phosphatidylethanolamines (PE)17:0/17:0, phosphatidylcholines (PC)17:0/17:0, sphingomyelins (SM) d18:1/17:0, triglycerides (TG) 17:0/17:0/17:0, ceramides (Cer) d18:1/17:0) and negative polar lipids (fatty acid (FA)17:0-d33), followed by the addition of ammonium acetate buffer (100 µL, 0.1 M, pH 4). After addition of methyl *tert*-butyl ether (1 mL), the tubes were thoroughly mixed for 4 min using a bullet blender

at medium speed (Next Advance), followed by a centrifugation step (5000 *g*, 12 min, 4 °C). Then 925 µL of the upper methyl tert-butyl ether layer was transferred into clean 1.5 mL Eppendorf tubes. Samples were dried in a speed-vac followed by reconstitution in acetonitrile/water (50 µL, 90/10, v/v). The reconstituted samples were centrifuged (14000 *g*, 3 min, 4 °C) before transferring into LC-MS vials. Each sample was injected on three different lipidomics platforms: endocannabinoids (5 µL), positive apolar lipids (2 µL) and for negative polar lipids (8 µL).

LC-MS/MS Analysis for endocannabinoids

A targeted analysis of 21 endocannabinoids and related *N*-acylethanolamines were measured using an Acquity UPLC I class Binary solvent manager pump (Waters) in conjugation with AB SCIEX 6500 quadrupole-ion trap (QTRAP) (AB Sciex). Separation was performed with Acquity HSS T3 column (1.2 x 100 mm, 1.8 µm) maintained at 45 °C. The aqueous mobile phase A consisted of 2 mM ammonium formate and 10 mM formic acid, and the organic mobile phase B was acetonitrile. The flow rate was set to 0.4 mL/min; initial gradient conditions were 55% B held for 2 min and linearly ramped to 100% B over 6 min and held for 2 min; after 10 s the system returned to initial conditions and held 2 min before next injection. Electrospray ionization-MS was operated in positive mode for measurement of 21 endocannabinoids and NAEs, and a selective Multiple Reaction Mode (sMRM) was used for quantification.

LC-MS/MS analysis for positive apolar and negative polar lipids

Both lipidomics methods are adapted and modified from previously published work[37]. In brief, these methods are measured on an Acquity UPLC Binary solvent manager pump (Waters) coupled to an Agilent 6530 electrospray ionization quadrupole time-of-flight (ESI-Q-TOF, Agilent, Jose, CA, USA) high resolution mass spectrometer using reference mass correction. The chromatographic separation was achieved on an Acquity HSS T3 column (1.2 x 100 mm, 1.8 µm) maintained at 40 °C for both methods. The positive polar lipids that include targets from different lipid classes including (lyso)phosphatidylcholines, triglycerides, ceramides. (Lyso)phosphatidylethanolamines and sphingomyelins were separated using a flow of 0.4 mL/min over a 16 min gradient. In positive mode, the aqueous mobile phase A consisted of 60/40 (v/v) acetonitrile/H_2O with 10 mM ammonium formate, and the organic mobile phase B consisted of 10/90 (v/v) acetonitrile/isopropanol with 10 mM ammonium formate. The negative apolar lipids that constitute mainly free fatty acids and (lyso)phosphatidylcholines were separated with a flow of 0.4 mL/min over 15 min gradient. In negative mode, the aqueous mobile phase A consisted of 5/95 (v/v) acetonitrile/H_2O with 10 mM ammonium formate, and the organic mobile phase B consisted of 99% (v/v) methanol with 10 mM Ammonium formate. The targets in both lipid methods were detected full scan (100-1000 m/z) in their respective ion charge mode.

Activity assays

Radiolabeled natural substrate assay FAAH

The radiolabeled natural substrate based assay for human FAAH was performed as reported previously[38]. Anandamide (AEA) (Sigma Chemical) was purchased from Sigma Chemical Co., purified FAAH was obtained from Cayman Chemical, [^{14}C-ethanolamine]-anandamide (60 Ci/mmol) was purchased from ARC. FAAH (2.5 µg per test) was pre-incubated with each compound (15 min, rt) and subsequently incubated with [^{14}C-ethanolamine]anandamide (10 µM, 15 min, 37 °C, in 500 µL of 50 mM Tris–HCl pH 9). The reaction was stopped by the addition of 0.6 mL of ice-cold methanol/chloroform (2:1, v/v). The mixture was centrifuged (3000 *g*, 5 min), the upper aqueous layer was put in a vial containing liquid scintillation cocktail (Ultima Gold XR, Perkin Elmer Life Sciences) and radioactivity was quantified in a β-counter.

Natural substrate-based fluorescence assay ABHD6

The natural substrate ABHD6 assay was performed as previously published[39].

Natural substrate-based fluorescence assay DAGLα/ß

The natural DAG substrate assay was performed as reported previously[17]. Standard assay conditions: 0.2 U/mL glycerol kinase (GK), glycerol-3-phosphate oxidase (GPO) and horseradish peroxidase (HRP), 0.125 mM ATP, 10 µM Amplifu™Red, 5% DMSO in a total volume of 200 µL. The assay additionally contained 5 µg/mL MGLL-overexpressing membranes, 100 µM SAG and 0.0075% (w/v) Triton X-100, with a final protein concentration of 50 µg/mL. The mDAGLβ assay was performed as the hDAGLα assay, but assay buffer was supplemented with 5 mM $CaCl_2$ and the SAG concentration was 75 µM.

Natural substrate-based fluorescence assay MGLL

The natural substrate MGLL assay was performed as previously published[17].

Surrogate substrate assay NAPE-PLD

The surrogate substrate assay was based on a previously reported method[40]. The membrane protein fraction of HEK293-T cells transiently overexpressing NAPE-PLD was diluted to 0.4 mg/mL in assay buffer (50 mM Tris-HCl pH 7.5, 0.02% Triton X-100, 150 mM NaCl). The substrate PED6 (10 mM, Invitrogen) was consecutively diluted in DMSO (25x) and in assay buffer (10x). The assay was performed in a dark Greiner 96 wells plate, end volume 100 µL. The membrane protein lysate (final concentration 0.04 mg/mL) was incubated with inhibitor or vehicle (30 min, 37 °C). A sample without membrane protein lysate was incorporated for background subtraction. Subsequently, substrate was added (PED6, final concentration: 1 µM) and the measurement is started immediately on a TECAN infinite M1000 pro (37 °C, scanning at 2 min intervals for 1 h: excitation 485 nm, emission 535 nm).

Radioligand displacement assays for cannabinoid receptors

[^{3}H]CP55940 displacement assays to determine the affinity for the CB1R and CB2R were performed as previously described[25,41], with the following changes. Ligands of interest were incubated (25 °C, 2 h) with membrane aliquots containing 1.5 µg (CHOK1hCB2_bgal) membrane protein in 100 µL assay buffer (50 mM Tris–HCl, 5 mM $MgCl_2$, 0.1% BSA, pH 7.4) with ~1.5 nM [^{3}H]CP55940 per assay point. Non-specific binding was determined in the presence of 10 µM AM630. Filtration was performed on 96-well GF/C filters, each well presoaked for 30 min with 25 µL 0.25% PEI, using a 96-wells Filtermate harvester (PerkinElmer). Filter-bound radioactivity was determined by scintillation spectrometry using a Microbeta® 2450 microplate counter (PerkinElmer).

Fluorescent Ca^{2+} assays for TRP ion channels

HEK293 (human embryonic kidney) cells stably overexpressing recombinant human TRPV1 or rat TRPA1, TRPV2, TRPV3, TRPV4, or TRPM8 were grown in 10 cm Petri dishes as mono-layers in minimum essential medium (MEM) supplemented with non-essential amino acids, 10% fetal bovine serum, 2 mM glutamine, and maintained at 5% CO_2 at 37 °C. Quantitative real time analysis was carried out to measure TRP gene over-expression in transfected-cells (data not shown). On the day of the experiment, cells were loaded with the methyl ester Fluo-4 AM in MEM (4 µM in DMSO containing 0.02% Pluronic F-127, Invitrogen (dark, 1 h, rt) washed twice with Tyrode's buffer (145 mM NaCl, 2.5 mM KCl, 1.5 mM $CaCl_2$, 1.2 mM $MgCl_2$, 10 mM d-glucose, and 10 mM HEPES, pH 7.4), resuspended in the same buffer and transferred (about 100,000 cells) to the quartz cuvette of the spectrofluorimeter (PerkinElmer LS50B equipped with PTP-1 Fluorescence Peltier System; PerkinElmer Life and Analytical Sciences) under continuous stirring. The effects on intracellular Ca^{2+} concentration ($[Ca^{2+}]_i$) before and after the addition of various concentrations of test compounds was measured by cell fluorescence (excitation: 488 nm, emission: 516 nm, 25 °C).

The effects of compounds were normalized against the response to ionomycin (4 µM) in each experiment. The increases in fluorescence in wildtype HEK293 cells were used as baseline and subtracted from the values obtained from transfected cells. Efficacy was defined as the maximum response elicited by the compounds tested and was determined by comparing their effect with the analogous effect observed with 4 µM ionomycin (Cayman), while the potency of the compounds (EC_{50}) was determined as the concentration required to produce half-maximal increases in $[Ca^{2+}]_i$. Curve fitting (sigmoidal dose–response variable slope) and parameter estimation were performed with GraphPad Prism 6 (GraphPad).

Antagonist/desensitizing behavior was evaluated by adding the test compounds in the quartz cuvette 5 min before stimulation of cells with agonists. In the case of human TRPV1-expressing HEK293 cells the agonist used was capsaicin (0.1 µM, in the case of SR141716A 10 nM was also used), which was able of elevating intracellular Ca^{2+} with a potency of EC_{50} = 5.3 ± 0.4 nM and efficacy = 78.6 ± 0.6%.

For TRPV2, the rat TRPV2-HEK293 cells exhibited a sharp increase in $[Ca^{2+}]_i$ upon application of lysophosphatidylcholine (LPC, 3 µM). The concentration for half-maximal activation was 3.40 ± 0.02 µM and efficacy was 91.7 ± 0.5%. For TRPV3, rat TRPV3-expressing HEK293 cells were first sensitized with the non-selective agonist 2-aminoethoxydiphenyl borate (100 µM). Antagonist/desensitizing behavior was evaluated against thymol (100 µM), which showed an efficacy of 34.7 ± 0.2% and a potency of EC_{50} = 84.1 ± 1.6 µM. For TRPV4, the rat TRPV4-expressing HEK293 cells the agonist used was *N*-((1*S*)-1-{[4-((2*S*)-2-{[(2,4-dichlorophenyl)sulfonyl]amino}-3-hydroxypropanoyl)-1-piperazinyl]carbonyl}-3-methylbutyl)-1-benzothiophene-2-carboxamide (GSK1016790A), (10 nM), which was able of elevating intracellular Ca^{2+} with a potency of EC_{50} = 0.46 ± 0.07 µM, and an efficacy of 51.9 ± 1.7%. For TRPM8, the rat TRPM8-expressing HEK293 cells, antagonist/desensitizing behavior was evaluated against icilin at 0.25 µM and 0.10 µM. For icilin, efficacy was 75.1 ± 1.1 and potency EC_{50} = 0.11 ± 0.01 µM. For HEK293 cells stably overexpressing recombinant rat TRPA1, the effects of TRPA1 agonists are expressed as a percentage of the effect obtained with 100 µM allyl isothiocyanate (AITC), which showed a potency of EC_{50} = 1.41 ± 0.04 µM and an efficacy of 65.9 ± 0.5.

The effect on $[Ca^{2+}]_i$ exerted by agonist alone was taken as 100%. Data are expressed as the concentration exerting a half-maximal inhibition of agonist-induced $[Ca^{2+}]_i$ elevation (IC_{50}), which was calculated again using GraphPad Prism 6 (Graphpad). All determinations were performed at least in triplicate. Statistical analysis of the data was performed by analysis of variance at each point using ANOVA followed by the Bonferroni's test.

Statistical methods

All statistical measures and methods are included in the respective figure or table captions. In brief: all data are shown as the mean ± SEM where applicable. A Student's *t*-test (unpaired, two-tailed) was used to determine differences between two groups. All statistical analyses were conducted using Excel (Microsoft) or GraphPad Prism 6 (Graphpad), and a p-value < 0.05 was considered significant throughout unless indicated otherwise. For the lipid profiling study (Figure 4E-F), a Benjamini-Hochberg correction (25% false discovery rate) was applied.

Supplementary data

Table S1 | Remaining enzyme activities of endocannabinoid related enzymes. DAGLα, DAGLβ, MGLL, ABHD6 and NAPE-PLD relative to DMSO as vehicle and [^{3}H]CP55940 displacement at overexpressing CB1R- and CB2R membranes (prefix h: human, prefix m: mouse).

Inhibitor		Remaining activity (% ± SD)					Radioligand displacement (% ± SEM)	
Protein:		hDAGLα	mDAGLβ	hMGLL	hABHD6	hNAPE-PLD	hCB1R	hCB2R
BIA 10-2474	10 µM	102.7 ± 9.3	94.1 ± 4.3	117.9 ± 3.0	83.9 ± 8.2	96.9 ± 11.9	29.8 ± 1.5	6.0 ± 5.4
	30 µM	113.4 ± 4.0	102.9 ± 1.9	-	31.2 ± 13.2	-	-	-
	50 µM	-	-	-	-	95.9 ± 10.1	38.4 ± 2.3	16.7 ± 8.9
BIA 10-2639	10 µM	107.6 ± 2.6	94.5 ± 1.7	-	111.2 ± 8.3	89.0 ± 7.2	36.8 ± 4.1	13.4 ± 8.0
	30 µM	110.2 ± 3.2	102.1 ± 4.2	-	90.3 ± 11.2	-	-	-
	50 µM	-	-	-	-	89.9 ± 2.6	44.0 ± 5.6	19.9 ± 5.4
PF044 57845	10 µM	99.2 ± 8.7	105.5 ± 0.5	-	108.3 ± 21.6	98.6 ± 6.7	59.9 ± 2.5	51.5 ± 4.6
	30 µM	83.0 ± 8.4	106.2 ± 1.5	-	97.5 ± 26.7	-	-	-
	50 µM	-	-	-	-	70.2 ± 6.8	103.8 ± 4.6	86.4 ± 1.3

Table S2 | Efficacy and affinity of compounds for TRPV-, TRPA1- and TRPM8-channels.

	TRPV1		TRPV2		TRPV3	
Inhibitor	Efficacy	IC_{50}	Efficacy	IC_{50}	Efficacy	IC_{50}
	% Ionomycin 4 µM	capsaicin 0.1 µM	% Ionomycin 4 µM	LPC 3 µM	% Ionomycin 4 µM	Thymol 100 µM
BIA 10-474	< 10	> 20 µM	< 10	> 20 µM	< 10	> 20 µM
PF04457845	< 10	> 20 µM	< 10	> 20 µM	< 10	> 20 µM
BIA 10-2639	< 10	> 20 µM	< 10	> 20 µM	< 10	> 20 µM

	TRPV4		TRPA1		TRPM8
Inhibitor	Efficacy	IC_{50}	Efficacy	IC_{50}	IC_{50}
	% ionomycin 4µM	GSK 10 nM	% AITC 100 µM	AITC 100 µM	Icilin 0.25 µM
BIA 10-2474	< 10	> 20 µM	< 10	> 20 µM	> 20 µM
PF04457845	< 10	> 20 µM	< 10	> 20 µM	> 20 µM
BIA 10-2639	< 10	> 20 µM	< 10	> 20 µM	> 20 µM

Table S3 | Lipids significantly altered by *in situ* BIA 10-2474 treatment of human cortical neurons. Lipids identified as significant based on *t*-test (with a post-hoc false discovery rate (FDR) correction applied using Benjamini-Hochberg procedure) and fold changes are divided into their different classes together with their trend. All lipids had an FDR rate less than 25%.

Lipid class	Metabolites identified as significant due to treatment	Effect
Phosphatidylcholines (PC)	C38:2, C38:6, C38:7, C40:6, C40:6, C40:7, C40:8	Increased
Lysophosphatidylcholines (LPC)	sn1&2: C14:0, C22:6, C16:0, C16:1, C18:0, C18:1, C18:2, C20:4 sn1: C18:2, C20:1, C20:2 C20:4, C22:6, C20:3 (ω3ω6) sn2: C14:0, C18:2, C20:4, C22:6, C20:3 (ω3ω6)	Increased
Fatty acids	C20:4 (ω6), C20:5 (ω3), C22:4, C25:5 (ω3ω6)	Decreased
Plasmalogen phosphatidylcholines (pPC)	C36:4, C36:6, C38:4, C38:5, C38:7, C40:6	Decreased
Triglycerides	C46:1, C48:1, C48:2, C48:3, C50:1, C52:1, C54:1	Increased
***N*-Acylethanolamines**	C20:4, C22:6, C18:1, C16:0, C16:1, C18:0	Increased
Mono&di-acylglycerols	sn1:C18:1, C18:2 & sn2: C18:1, C18:2	Increased
Sphingomyelins	C18:1/24:1	Increased

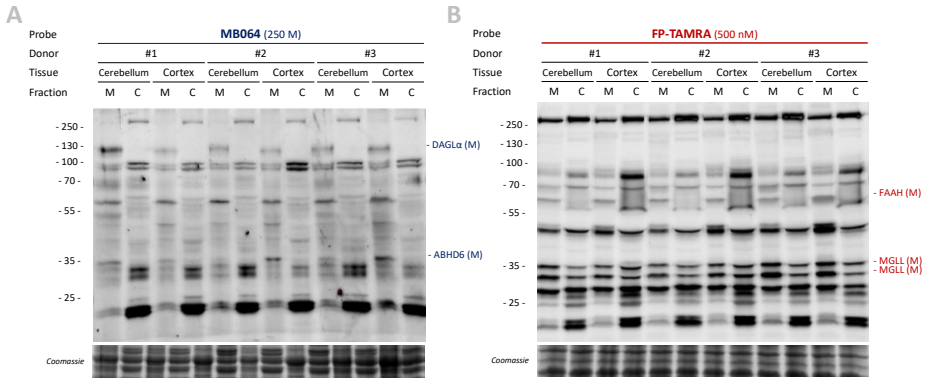

Figure S1 | Serine hydrolase profiling in human brain proteome by comparative ABPP. (**A**-**B**) Labeling comparison between human cerebellum and cortex, membrane (M) and cytosol (C) fractions of three independent donors. Human proteome was labeled with MB064 (250 nM) (**A**) or FP-TAMRA (500 nM) (**B**) (20 min, rt).

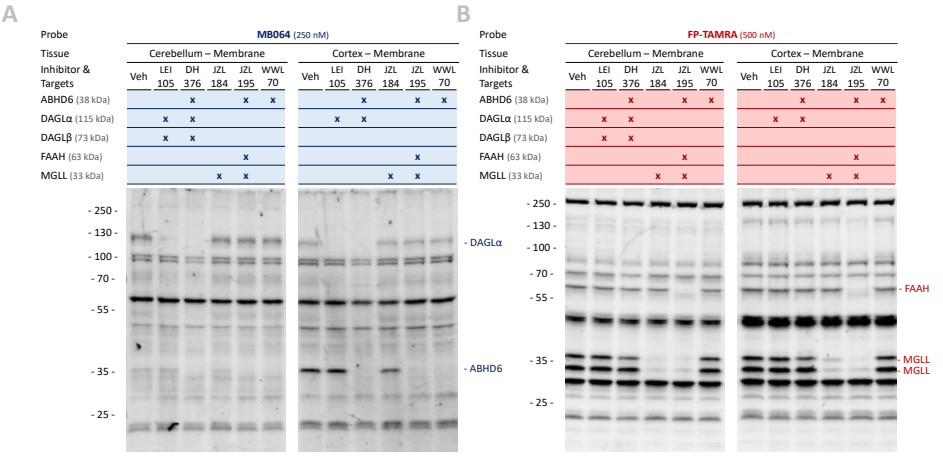

Figure S2 | Band identification in human brain proteome by competitive ABPP. (**A**-**B**) Human proteome (cerebellum and cortex, membrane fraction) was incubated with vehicle or reference inhibitors LEI105[14], DH376[25], JZL184[42], JZL195[8], WWL70[43] (10 µM, 30 min, 37 °C) and subsequently labeled with MB064 (250 nM) (**A**) or FP-TAMRA (500 nM) (**B**) (20 min, rt). Inhibitor targets and identified bands are indicated in the figure.

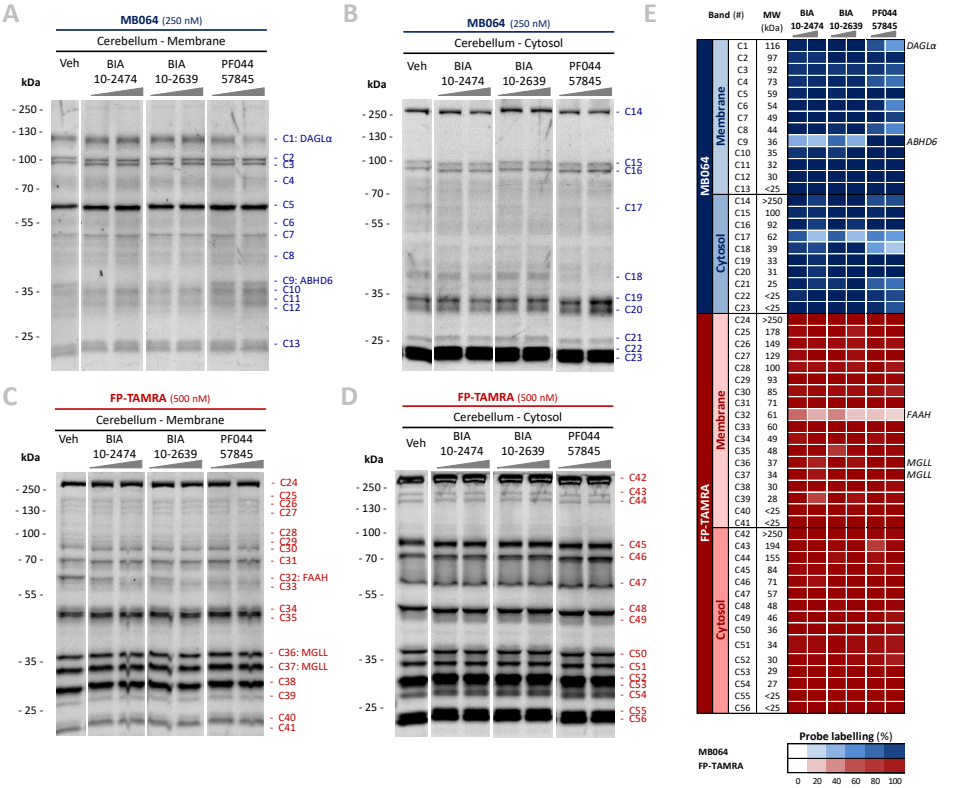

Figure S3 | Identification of FAAH and ABHD6 as *in vitro* targets of BIA 10-2474 by competitive ABPP on serine hydrolases. Gel-based ABPP analysis of human cerebellum proteome incubated *in vitro* with vehicle or inhibitor BIA 10-2474, BIA 10-2639 or PF04457845 (10/50 µM, 30 min, 37 °C) and subsequently labeled with MB064 (250 nM) (**A**,-**B**) or FP-TAMRA (500 nM) (**B**, **D**) (20 min, rt). (**E**) Heat-map summary of all 56 quantified bands, normalized for protein loading and expressed relative to control (n=3).

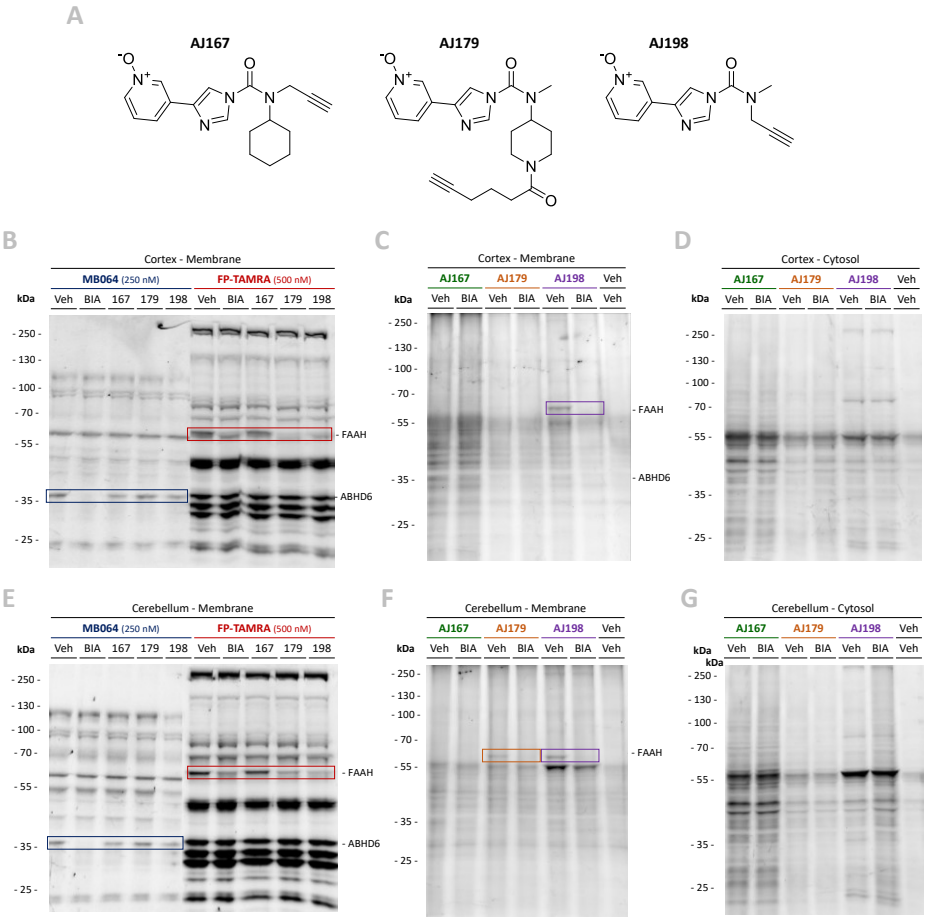

Figure S4 | BIA 10-2474 interaction profiling by two-step labeling of human cortex and cerebellum with BIA-derived two-step probes. (**A**) Chemical structures of BIA 10-2474 derived two-step probes AJ167, AJ179, and AJ198. (**B**, **E**) Two-step probe validation by competitive ABPP with BIA 10-2474 and AJ167, AJ179, AJ198. Human cortex (**B**) or cerebellum (**E**) membranes were incubated with vehicle, BIA 10-2474, or two-step probe (50 µM, 30 min, 37 °C) and subsequently labeled with MB064 (250 nM) or FP-TAMRA (500 nM) (20 min, rt). (**C**-**D**, **F**-**G**) Competitive two-step ABPP with BIA 10-2474 and two-step probes. Human cortex (**C**-**D**) or cerebellum (**F**-**G**) proteome was incubated *in vitro* with vehicle or BIA 10-2474 (50 µM, 30 min, 37 °C) and subsequently labeled with two step probe (AJ167, AJ179 or AJ198) (50 µM, 30 min, 37 °C). Cy5-azide was conjugated to the bound probe by copper-catalyzed click reaction.

References

1. Eddleston, M., Cohen, A. F. & Webb, D. J. Implications of the BIA-102474-101 study for review of first-into-human clinical trials. *British Journal of Clinical Pharmacology* **81,** 582–586 (2016).
2. Butler, D. & Callaway, E. Scientists in the dark after French clinical trial proves fatal. *Nature* **529,** 263–264 (2016).
3. Kerbrat, A. *et al.* Acute Neurologic Disorder from an Inhibitor of Fatty Acid Amide Hydrolase. *N. Engl. J. Med.* **375,** 1717–1725 (2016).
4. Bégaud, B. *et al.* BIA 10-2474: Minutes of the Temporary Specialist Scientific Committee (TSSC) meeting on 'FAAH (Fatty Acid Amide Hydrolase) Inhibitors'. *Meet. Minutes* 1–14 (2016).
5. Cravatt, B. F. *et al.* Molecular characterization of an enzyme that degrades neuromodulatory fatty-acid amides. *Nature* **384,** 83–87 (1996).
6. Kathuria, S. *et al.* Modulation of anxiety through blockade of anandamide hydrolysis. *Nat. Med.* **9,** 76–81 (2003).
7. Devane, W. A. *et al.* Isolation and structure of a brain constituent that binds to the cannabinoid receptor. *Science (80-.).* **258,** 1946–1949 (1992).
8. Long, J. Z. *et al.* Dual blockade of FAAH and MAGL identifies behavioral processes regulated by endocannabinoid crosstalk in vivo. *Proc. Natl. Acad. Sci. U. S. A.* **106,** 20270–5 (2009).
9. Van Der Stelt, M. *et al.* Anandamide acts as an intracellular messenger amplifying Ca2+ influx via TRPV1 channels. *EMBO J.* **24,** 3026–3037 (2005).
10. Hampson, A. J. *et al.* Dual Effects of Anandamide on NMDA Receptor-Mediated Responses and Neurotransmission. *J. Neurochem.* **70,** 671–676 (2002).
11. Huggins, J. P., Smart, T. S., Langman, S., Taylor, L. & Young, T. An efficient randomised, placebo-controlled clinical trial with the irreversible fatty acid amide hydrolase-1 inhibitor PF-04457845, which modulates endocannabinoids but fails to induce effective analgesia in patients with pain due to osteoarthritis of th. *Pain* **153,** 1837–1846 (2012).
12. Li, G. L. *et al.* Assessment of the pharmacology and tolerability of PF-04457845, an irreversible inhibitor of fatty acid amide hydrolase-1, in healthy subjects. *Br. J. Clin. Pharmacol.* **73,** 706–716 (2012).
13. Niphakis, M. J. & Cravatt, B. F. Enzyme Inhibitor Discovery by Activity-Based Protein Profiling. *Annu. Rev. Biochem.* **83,** 341–377 (2014).
14. Baggelaar, M. P. *et al.* Highly Selective, Reversible Inhibitor Identified by Comparative Chemoproteomics Modulates Diacylglycerol Lipase Activity in Neurons. *J. Am. Chem. Soc.* **137,** 8851–8857 (2015).
15. Liu, Y., Patricelli, M. P. & Cravatt, B. F. Activity-based protein profiling: The serine hydrolases. *Proc. Natl. Acad. Sci.* **96,** 14694–14699 (1999).
16. Ahn, K. *et al.* Mechanistic and Pharmacological Characterization of PF-04457845: A Highly Potent and Selective Fatty Acid Amide Hydrolase Inhibitor That Reduces Inflammatory and Noninflammatory Pain. *J. Pharmacol. Exp. Ther.* **338,** 114–124 (2011).
17. van der Wel, T. *et al.* A natural substrate-based fluorescence assay for inhibitor screening on diacylglycerol lipase α. *J. Lipid Res.* **56,** 927–935 (2015).
18. Van Esbroeck, A. C. M. *et al.* Activity-based protein profiling reveals off-target proteins of the FAAH inhibitor BIA 10-2474. *Science (80-.).* **356,** 1084–1087 (2017).
19. Rostovtsev, V. V., Green, L. G., Fokin, V. V. & Sharpless, K. B. A stepwise huisgen cycloaddition process: Copper(I)-catalyzed regioselective 'ligation' of azides and terminal alkynes. *Angew. Chemie - Int. Ed.* **41,** 2596–2599 (2002).
20. Wei, B. Q., Mikkelsen, T. S., McKinney, M. K., Lander, E. S. & Cravatt, B. F. A second fatty acid amide hydrolase with variable distribution among placental mammals. *J. Biol. Chem.* **281,** 36569–36578 (2006).

21. Lanning, B. R. *et al.* A road map to evaluate the proteome-wide selectivity of covalent kinase inhibitors. *Nat. Chem. Biol.* **10,** 760–767 (2014).
22. Thomas, G. *et al.* The Serine Hydrolase ABHD6 Is a Critical Regulator of the Metabolic Syndrome. *Cell Rep.* **5,** 508–520 (2013).
23. Chang, P. A. & Wu, Y. J. Neuropathy target esterase: An essential enzyme for neural development and axonal maintenance. *International Journal of Biochemistry and Cell Biology* **42,** 573–575 (2010).
24. Baggelaar, M. P. *et al.* Development of an activity-based probe and in silico design reveal highly selective inhibitors for diacylglycerol lipase-α in brain. *Angew. Chemie - Int. Ed.* **52,** 12081–12085 (2013).
25. Ogasawara, D. *et al.* Rapid and profound rewiring of brain lipid signaling networks by acute diacylglycerol lipase inhibition. *Proc. Natl. Acad. Sci.* **113,** 26–33 (2016).
26. Li, Y. *et al.* Carboxylesterase 2 prevents liver steatosis by modulating lipolysis, endoplasmic reticulum stress, and lipogenesis and is regulated by hepatocyte nuclear factor 4 alpha in mice. *Hepatology* **63,** 1860–1874 (2016).
27. Shayman, J. A. & Abe, A. Drug induced phospholipidosis: An acquired lysosomal storage disorder. *Biochim. Biophys. Acta - Mol. Cell Biol. Lipids* **1831,** 602–611 (2013).
28. Blankman, J. L., Simon, G. M. & Cravatt, B. F. A comprehensive profile of brain enzymes that hydrolyze the endocannabinoid 2-arachidonoylglycerol. *Chem. Biol.* **14,** 1347–1356 (2007).
29. Pribasnig, M. A. *et al.* α/β hydrolase domain-containing 6 (ABHD6) degrades the late Endosomal/Lysosomal lipid Bis(Monoacylglycero)phosphate. *J. Biol. Chem.* **290,** 29869–29881 (2015).
30. Wei, M. *et al.* α/β-Hydrolase domain-containing 6 (ABHD6) negatively regulates the surface delivery and synaptic function of AMPA receptors. *Proc. Natl. Acad. Sci.* **113,** E2695–E2704 (2016).
31. Erlenhardt, N. *et al.* Porcupine Controls Hippocampal AMPAR Levels, Composition, and Synaptic Transmission. *Cell Rep.* **14,** 782–794 (2016).
32. Kolter, T. & Wendeler, M. Chemical chaperones - A new concept in drug research. *ChemBioChem* **4,** 260–264 (2003).
33. Richardson, R. J., Hein, N. D., Wijeyesakere, S. J., Fink, J. K. & Makhaeva, G. F. Neuropathy target esterase (NTE): Overview and future. in *Chemico-Biological Interactions* **203,** 238–244 (2013).
34. Read, D. J., Li, Y., Chao, M. V, Cavanagh, J. B. & Glynn, P. Neuropathy Target Esterase Is Required for Adult Vertebrate Axon Maintenance. *J. Neurosci.* **29,** 11594–11600 (2009).
35. Moser, M. *et al.* Cloning and expression of the murine sws/NTE gene. *Mech. Dev.* **90,** 279–282 (2000).
36. Bachovchin, D. A. *et al.* Superfamily-wide portrait of serine hydrolase inhibition achieved by library-versus-library screening. *Proc. Natl. Acad. Sci.* **107,** 20941–20946 (2010).
37. Hu, C. *et al.* RPLC-Ion-trap-FTMS method for lipid profiling of plasma: Method validation And application to p53 mutant mouse model. *J. Proteome Res.* **7,** 4982–4991 (2008).
38. Gattinoni, S. *et al.* Enol carbamates as inhibitors of fatty acid amide hydrolase (FAAH) endowed with high selectivity for FAAH over the other targets of the endocannabinoid system. *ChemMedChem* **5,** 357–360 (2010).
39. Janssen, F. J. *et al.* Discovery of glycine sulfonamides as dual inhibitors of sn-1-diacylglycerol lipase α and α/β-hydrolase domain 6. *J. Med. Chem.* **57,** 6610–6622 (2014).
40. Peppard, J. V., Mehdi, S., Li, Z. & Duguid, M. S. Assay methods for identifying agents that modify the activity of nape-pld or Abhd4. (2010).
41. Mukhopadhyay, P. *et al.* The novel, orally available and peripherally restricted selective cannabinoid CB2receptor agonist LEI-101 prevents cisplatin-induced nephrotoxicity. *Br. J. Pharmacol.* **173,** 446–458 (2016).

42. Long, J. Z. *et al.* Selective blockade of 2-arachidonoylglycerol hydrolysis produces cannabinoid behavioral effects. *Nat. Chem. Biol.* **5,** 37–44 (2009).
43. Li, W., Blankman, J. L. & Cravatt, B. F. A functional proteomic strategy to discover inhibitors for uncharacterized hydrolases. *J. Am. Chem. Soc.* **129,** 9594–9595 (2007).